The Astrophysical Journal Supplement Series, 242:6 (10pp), 2019 May https://doi.org/10.3847/1538-4365/ab13b8

Physical Parameters of Northern Eclipsing Binaries in the Catalina Sky Survey

Athanasios Papageorgiou[1,2], Márcio Catelan[1,2,3,6], Panagiota-Eleftheria Christopoulou[4], Andrew J. Drake[5], and S. G. Djorgovski[5]

[1] Pontificia Universidad Católica de Chile, Facultad de Física, Instituto de Astrofísica, Av. Vicuña Mackenna 4860, 7820436 Macul, Santiago, Chile
apapageo@astro.puc.cl
[2] Millennium Institute of Astrophysics, Santiago, Chile
[3] Centro de Astro-Ingeniería, Pontificia Universidad Católica de Chile, Av. Vicuña Mackenna 4860, 7820436 Macul, Santiago, Chile
[4] Department of Physics, University of Patras, 26500, Patra, Greece
[5] California Institute of Technology, 1200 East California Boulevard, Pasadena, CA 91225, USA
Received 2018 December 12; revised 2019 March 16; accepted 2019 March 25; published 2019 May 8

Abstract

We present the physical properties for 2281 northern eclipsing binary (EB) stars with eclipsing Algol (EA)-type light-curve (LC) morphology, based on data extracted from the Catalina Sky Survey (CSS). Our study is based on the analysis of the Eclipsing Binary via Artificial Intelligence (EBAI) artificial neural network (ANN) tool. An intensive search for the optimal ANN topology was performed. In order to feed the ANN with LCs that are representative of the CSS observations, two independent methods, based on template fitting and on the Two-Gaussian Model, were applied. As a result, five principal physical parameters were determined using only the CSS LCs, namely the temperature ratio, $\frac{T_2}{T_1}$; the sum of relative radii, $\rho_2 + \rho_1$; $e \sin\omega$; $e \cos\omega$; and $\sin i$, where e is the eccentricity, ω is the argument of periastron, and i is the orbital inclination. Parameter uncertainties were estimated based on a Monte Carlo approach. When the ANN predictions were out of its training limits (1540 EBs), the parameters of the systems are based on the matching templates technique only. The results are fully in agreement with the expected parameter values for detached EB systems and can be used as initial inputs for advanced and dedicated EB models and/or for statistical purposes.

Key words: binaries: eclipsing – methods: data analysis – stars: fundamental parameters

Supporting material: machine-readable tables

1. Introduction

There is no doubt that eclipsing binaries (hereafter EBs), and specifically detached double-lined EBs without mass transfer, are forerunners in modern stellar astrophysics. Not only do they provide the prime tool for the validation of the current stellar structure and evolution models but also a wealth of fundamental information that ultimately contributes to our understanding of the structure and evolution of galaxies, including our own (Hełminiak et al. 2013; Pietrzyński et al. 2013; Graczyk et al. 2014). In the last few decades, a long list of astronomical sky surveys enriched the astronomical databases with not only a huge amount of newly discovered EBs, but also with higher photometric precision and different wavelengths in a wide range of magnitudes, including, for instance, Kepler (Kirk et al. 2016) and the *Wide-field Infrared Survey Explorer* (*WISE*; Chen et al. 2018). This trend will continue and expand in the future, particularly with the start of operations of the Large Synoptic Survey Telescope (LSST; Prša et al. 2011b). For the exploration and study of the information from these increasingly large data sets, it has become increasingly clear that automated methods and machine-learning algorithms are needed. Such techniques have been applied in large data volumes in order to classify and/or extract the physical properties of EBs in particular. Following the estimations in Prša et al. (2011b), a manual approach to light-curve (LC) modeling for the analysis of EBs cannot continue into the LSST era.

The Eclipsing Binary via Artificial Intelligence tool (EBAI; Prša et al. 2008; Guinan et al. 2009) is a three-layer back-propagating artificial neural network (ANN) that yields the principal parameters of eclipsing binaries. EBAI has been tested on 50 EBs from the Catalog and Atlas of Eclipsing Binaries (CALEB[7]) database. Using this tool, 2580 EBs (Wyrzykowski et al. 2003) were classified as detached based on data from the Optical Gravitational Lensing Experiment (OGLE; Udalski et al. 1992) and had their physical parameters estimated with remarkable success, based solely on the geometrical characteristics of their LCs. A total of 1879 EBs from the Kepler mission (Prša et al. 2011a) were also analyzed using the EBAI ANN, and their physical parameters were extracted from their LCs. More recently, Yang et al. (2015) employed the EBAI pipeline to calculate the physical parameters of 50 EBs observed with the Chinese Small Telescope ARray (CSTAR). In spite of these successful applications, it must be kept in mind that only some of the physical parameters can be extracted from the LCs, namely those that have a significant effect on the LC and differ between EB subtypes.

In this paper, physical parameters for 2281 EBs detected by the Catalina Sky Survey (CSS; Larson et al. 2003; Drake et al. 2009) are estimated using the EBAI ANN. The paper is organized as follows. In Section 2, we briefly describe the CSS data that we use in our analysis, as well as the methods we used to fit the data. Section 3 presents the construction of the training/validation sets, the parameter optimization of the ANN, the validation, and recognition procedures. In Section 4,

[6] On sabbatical leave at the European Southern Observatory, Av. Alonso de Córdova 3107, 7630355 Vitacura, Santiago, Chile.

[7] http://caleb.eastern.edu

Table 1
Eclipsing Binary Systems in CSS

Name	ID	R.A. (h:m:s)	Decl. (°: ′: ″)	Flag
CSS_J235856.7+371823	1138103019678	23:58:56.76	+37:18:23.5	TMPL+TGM
CSS_J235715.5+305455	1129113073931	23:57:15.56	+30:54:55.4	TGM
CSS_J235444.8+305751	1129113076324	23:54:44.84	+30:57:51.9	TGM
CSS_J235227.0+395515	1140099013325	23:52:27.04	+39:55:15.3	TGM
CSS_J235151.3+035409	1104128021471	23:51:51.32	+03:54:09.0	TMPL+TGM
CSS_J235104.0+115651	1112126013602	23:51:04.05	+11:56:51.3	TGM
CSS_J234850.3+133300	1112126046557	23:48:50.32	+13:33:00.1	TGM
CSS_J234826.5+271203	1126116047239	23:48:26.59	+27:12:03.6	TMPL+TGM
CSS_J234734.4+203331	1121120017534	23:47:34.40	+20:33:31.9	TMPL+TGM
CSS_J234700.0+180015	1118122023624	23:47:00.04	+18:00:15.6	TGM
CSS_J234554.3−003131	1001127046283	23:45:54.31	−00:31:31.1	TMPL+TGM
CSS_J234502.5+415419	1140098084200	23:45:02.59	+41:54:19.9	TGM
CSS_J234348.2+270630	1126115046718	23:43:48.29	+27:06:30.4	TGM
CSS_J234331.2−010354	1001127036441	23:43:31.21	−01:03:54.4	TMPL+TGM
CSS_J234306.1+060347	1107126008187	23:43:06.11	+06:03:47.7	TMPL+TGM
CSS_J233925.0+301419	1129112053480	23:39:25.01	+30:14:19.6	TMPL+TGM
CSS_J233903.3+244754	1123117054880	23:39:03.35	+24:47:54.8	TMPL+TGM
CSS_J233902.7+364733	1138102003558	23:39:02.79	+36:47:33.7	TMPL+TGM
CSS_J233834.6+180614	1118122025827	23:38:34.63	+18:06:14.0	TMPL+TGM
CSS_J233714.0+324147	1132109046798	23:37:14.07	+32:41:47.4	TMPL+TGM
CSS_J233651.3+353158	1135105051320	23:36:51.30	+35:31:58.9	TMPL+TGM
CSS_J233608.6+344712	1135105028344	23:36:08.68	+34:47:12.8	TMPL+TGM
CSS_J233511.5+003256	1101126011082	23:35:11.53	+00:32:56.2	TMPL+TGM
CSS_J233440.6+415531	1140098085030	23:34:40.63	+41:55:31.4	TGM
CSS_J233313.7+283745	1129111011824	23:33:13.71	+28:37:45.5	TMPL+TGM
CSS_J233159.8+132745	1112124044517	23:31:59.86	+13:27:45.9	TMPL+TGM
CSS_J233133.0+141548	1115122003657	23:31:33.09	+14:15:48.8	TGM
CSS_J233116.3+324003	1132108047623	23:31:16.37	+32:40:03.5	TMPL+TGM

(This table is available in its entirety in machine-readable form.)

we discuss our results, followed by a brief summary of our work in Section 5.

2. Data Selection and Preprocessing

In this study, we focus on the Catalina Surveys Data Release 2[8] (CSDR2), which was described by Drake et al. (2014) and more recently, in the specific context of EB systems, by Papageorgiou et al. (2018). This includes a total of 4683 EBs originally classified either as eclipsing Algol (EA) -type systems (using 8 yr of data; Drake et al. 2014) or detached/semi-detached systems (using data spanning 12 yr; Papageorgiou et al. 2018). The EBs cover a region of R.A. between 0 and 24 hr and decl. between −22° and +65° (Table 1). The observations are taken unfiltered, and the magnitudes are transformed to an approximate V magnitude ($V_{\rm CSS}$; Drake et al. 2013). The photometry was performed using the aperture photometry program SExtractor (Bertin & Arnouts 1996). Blending is limited to a small percentage of sources because the telescope avoids the Galactic plane region by 10°–15° and the CSS pixel size is 2.″5 in the 4k charged coupled device data. The original CSS photometric errors are significantly overestimated, as discussed in Graham et al. (2017) who provide a corrective factor to compensate for this problem. For these 4680 EBs, after applying a series of period-finding methods, Papageorgiou et al. (2018) presented a catalog with improved periods and a mean magnitude error (see their Table 1) but also with phenomenological parameters (see their Table 2) of their LCs.

The EBAI ANN uses normalized and equidistant phased LCs as inputs. However, the observed LCs have gaps and generally are not uniformly sampled. Thus, in order to create a representative LC for each EB system, we used different approximations such as polynomial chain fitter (Prša et al. 2008), phenomenological models (Mikulášek 2015), template fitting (TMPL; Layden 1998), and the Two-Gaussian Model (TGM; Mowlavi et al. 2017). In the following subsections, we present the TMPL and TGM methods, which had the best performance in our data set.

2.1. TMPL Fitting

The principal parameters that can affect the shape of an LC are the temperature ratio, $\frac{T_2}{T_1}$; the sum of relative radii, $\rho_2 + \rho_1$; $e\sin\omega$; $e\cos\omega$; and $\sin i$, where e is the eccentricity, ω is the argument of periastron, and i is the orbital inclination. Using a Monte Carlo–based script in the PHysics Of Eclipsing BinariEs (PHOEBE)-scripter (Prša & Zwitter 2005), a large database of ∼84,000 detached and semi-detached LCs in the Johnson V band was generated. This was done by randomly selecting $\frac{T_2}{T_1}$ from a half-Gaussian distribution and $\rho_2 + \rho_1$ from a uniform distribution, whereas $e\sin\omega$ and $e\cos\omega$ were selected from exponential distributions. Finally, $\sin i$ was selected from a uniform distribution in inclination, but with a built-in cut-off point in order to ensure the occurrence of eclipses (Prša et al. 2008).

[8] http://nesssi.cacr.caltech.edu/DataRelease/

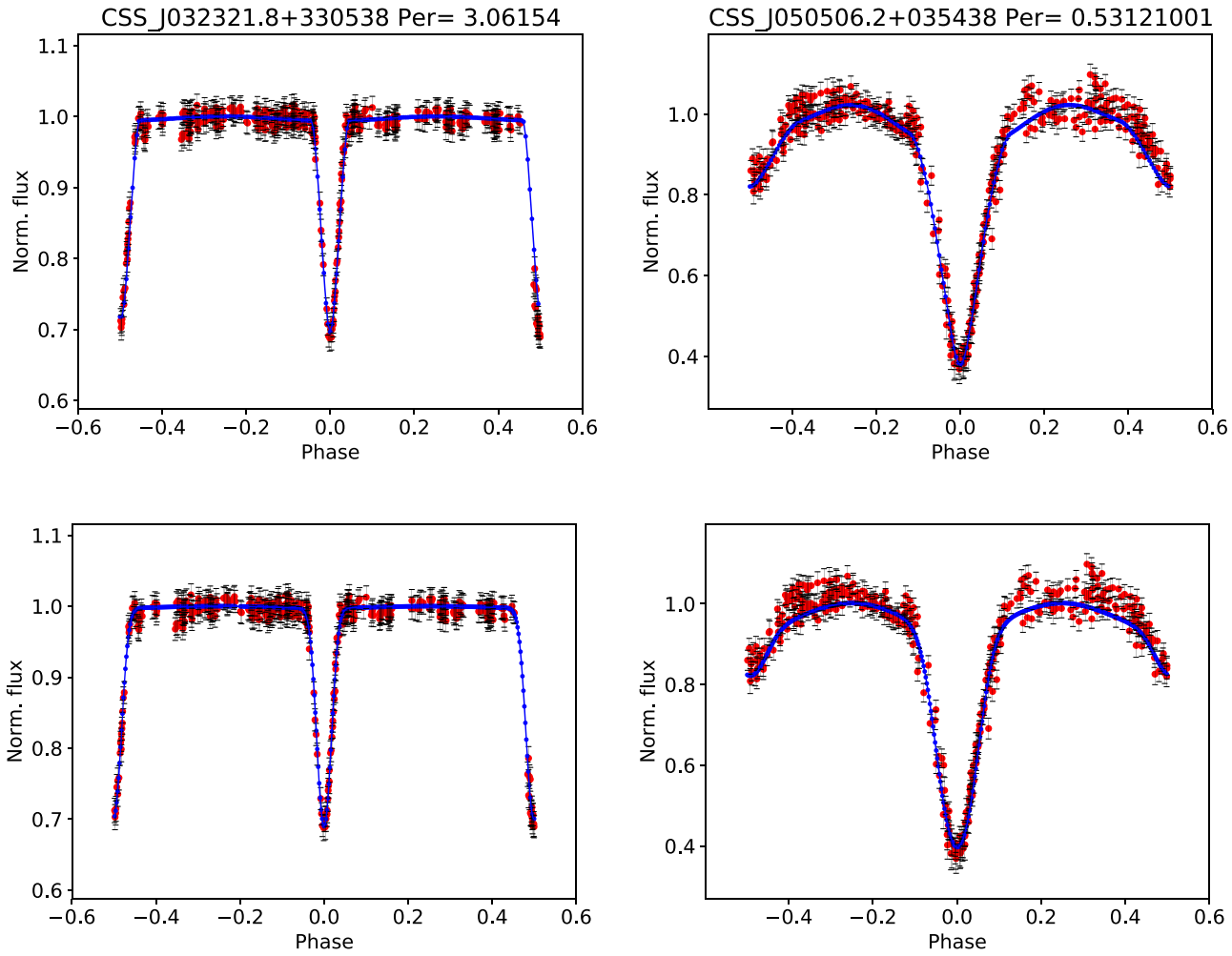

Figure 1. Representative examples of detached (left) and semi-detached (right) EB fits, using the TMPL (top) and TGM (bottom) methods. The headers denote the CSS name and the period (in days).

Based on Layden's TMPL method (Layden 1998), a parallel code in Python was developed. First, the available LCs are distributed among the computing units in order to reduce the execution time. Each unit matches the observed LCs with the template database, and the best synthetic LC is returned based on the χ^2 statistic, followed by the set of parameters and the classification type of the template LC. A reasonable fit was thus achieved for 3211 out of the 4683 LCs in the original sample (Figure 1, top). For the remaining LCs, visual inspection ultimately revealed that the fits were not satisfactory, and they were accordingly discarded. Such unsatisfactory fits were produced mostly by noisy or asymmetric LCs (probably due to spot activity) and/or the absence/limited number of photometric data points during eclipses.

2.2. TGM Fitting

TGM is constructed using Gaussian functions to model the eclipses and a cosine function to model ellipsoidal variability (if present). The TGM parameters include the phases, the half widths, and the depths of the primary and secondary eclipses, the peak-to-peak amplitude of the ellipsoidal-like variation, and a constant that equals the maximum light of the LC in the case of detached systems. We adopted the phenomenological models described in Papageorgiou et al. (2018) for 4050 LCs from CSS (Figure 1, bottom).

2.3. Comparison between TMPL and TGM Results

For 2845 LCs, we were able to obtain successful fits using both the TMPL (Section 2.1) and TGM (Section 2.2) methods. This gives us the opportunity to estimate the physical parameters from two independent approximations of the original LCs. The mean percentage difference between the two methods per LC for the whole phase range [0, 1] is $\sim$0.65%.

3. EBAI Performance on CSS Data

3.1. The Training and Validation Sets

Using the TMPL method, it is possible to estimate the parameters of the EBs based on the best-fitting LCs, although morphologically similar LCs could lead to degenerate solutions. In order to minimize this problem, we also employed an EBAI ANN (Prša et al. 2008) on the fitted LCs. Following the method proposed by Prša et al. (2008), the five aforementioned fundamental physical parameters can be derived from such an ANN, namely $\frac{T_2}{T_1}$, $\rho_2 + \rho_1$, $e \sin\omega$, $e \cos\omega$, and $\sin i$ (see Section 2.1). First, a set of 49,000 LCs of detached and semi-detached EBs were generated in the V band using PHOEBE

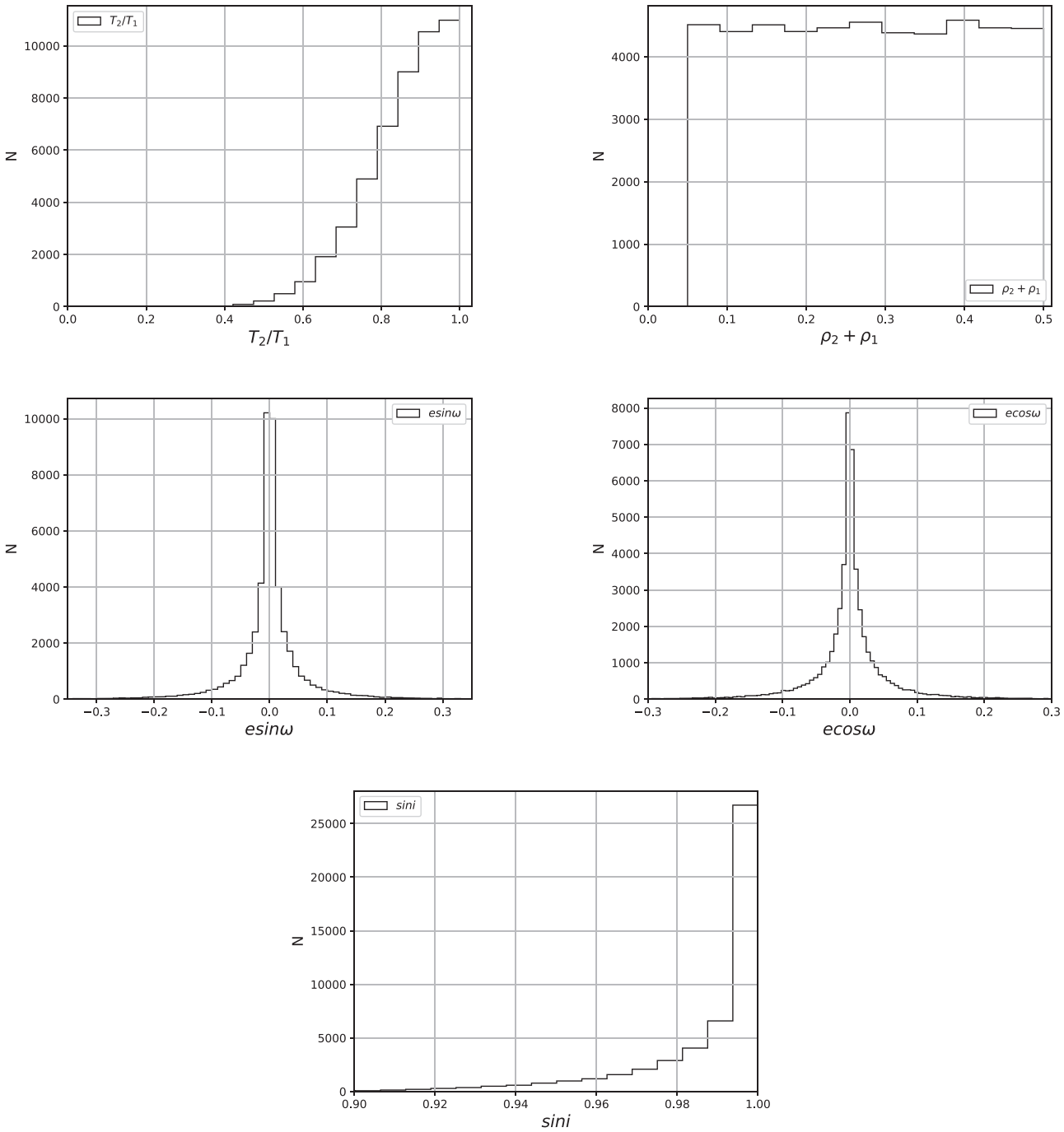

Figure 2. Training set parameter distributions, as generated for use with the TMPL fitting method (Section 2.1).

(Prša & Zwitter 2005) for the training procedure.[9] An additional 20,000 LCs were similarly generated for the validation procedure. In order to eliminate the systematics, the synthesis of the LCs for the training and validation was done using a Monte Carlo script in PHOEBE, sampling the parameters randomly according to the distributions functions described in Section 2.1 (Figure 2). The training and validation LCs were constructed with 201 points, which were equidistant in phase over the phase range [−0.5, 0.5]. The script used to generate the training and validation sets interpopulates limb darkening coefficients from van Hamme (1993) tables for the given temperatures and applies the changes to the synthetic LCs. The gravity darkening exponent was accordingly applied to the models.

3.2. ANN Optimization

For the optimization of the ANN, different topologies were tested, varying the numbers of hidden nodes in the range of [20–190] with a step of 10 hidden nodes. Each topology was trained for 500,000 iterations. Figure 3 (left) presents the cost function value (CFV) during the training of the different network topologies. The best network topologies were found in

[9] Given that the training is performed on PHOEBE models, it should be kept in mind that all uncertainties and approximations that are inherent to those models are implicitly propagated to the solutions, when the method is used to infer the parameters of real EB LCs.

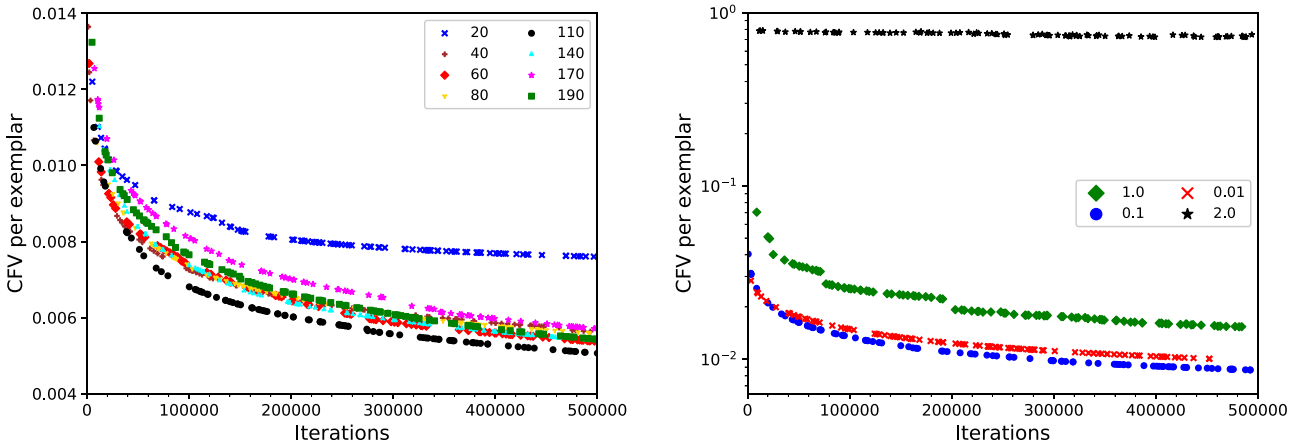

Figure 3. (Left) CFV as a function of the number of iterations during the training on different network topologies. The number of hidden nodes used in each case is indicated in the inset. (Right) As in the left panel, but for learning rate parameter values of 0.01, 0.1, 1.0, and 2.0, again as indicated in the inset, and assuming 110 hidden nodes.

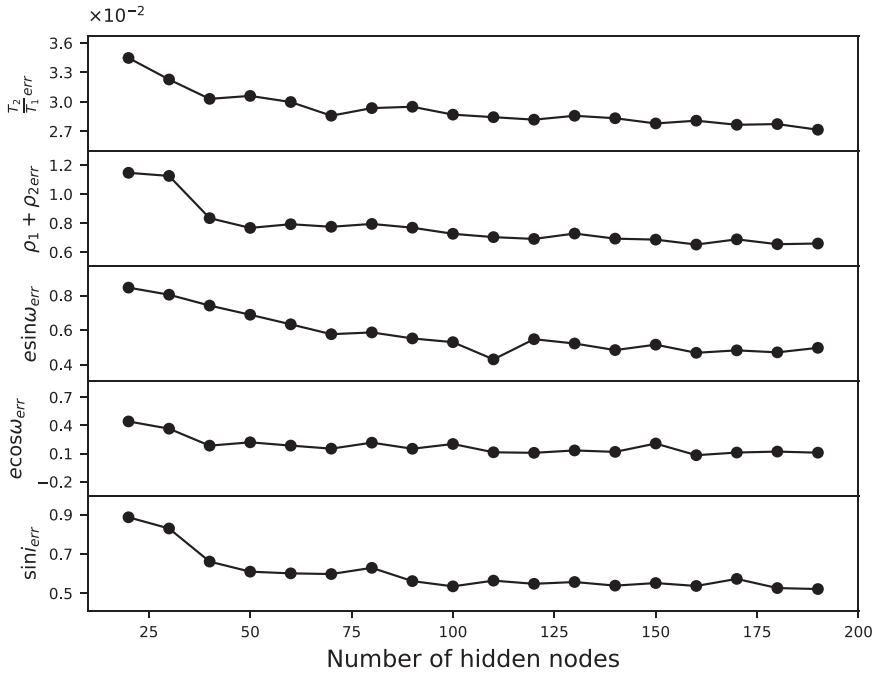

Figure 4. Searching for the optimum topology of the ANN: the rms error of the parameters (from top to bottom) are $\frac{T_2}{T_1}$, $\rho_2 + \rho_1$, $e \sin\omega$, $e \cos\omega$, and $\sin i$ for different numbers of hidden nodes.

the range of 100–130 hidden nodes. The value of 110 hidden nodes was adopted for the final ANN topology (Figure 4). The best value of the learning rate parameter was found by testing different values in the range [0.01–2.0]. Figure 3 (right) presents the CFV with the number of iterations for the learning rate values of 0.01, 0.1, 1.0, and 2.0. Best results (a smaller CFV for a given number of iterations) were obtained with a learning rate parameter of 0.1, which was adopted for the final ANN topology and was held fixed during the actual learning process.

3.3. Final ANN Training and Validation

The optimized ANN parameters from Section 3.2 were adopted, and the final training was performed for 1.5 million iterations, using 25 cores on the Geryon 2 supercomputer hosted at the Pontificia Universidad Católica de Chile's Institute of Astrophysics and Astro-Engineering Center. A jitter of 0.5% was added to the ANN input during the final training. Figure 5 shows the actual parameter values of the validation set of 20,000 synthetic LCs versus the output parameter values calculated from the EBAI code. More than 90% of the sample has errors in all five parameters that are smaller than 10%. Note that, in order to estimate the sensitivity of EBAI on small variations, during the recognition phase of both TGM and TMPL models, we added variable random noise at the level of 1% to each representative LC data point, whereupon the parameter values were recalculated. The mean value and standard deviation were thus computed for the different LC parameters after 1000 recognitions.

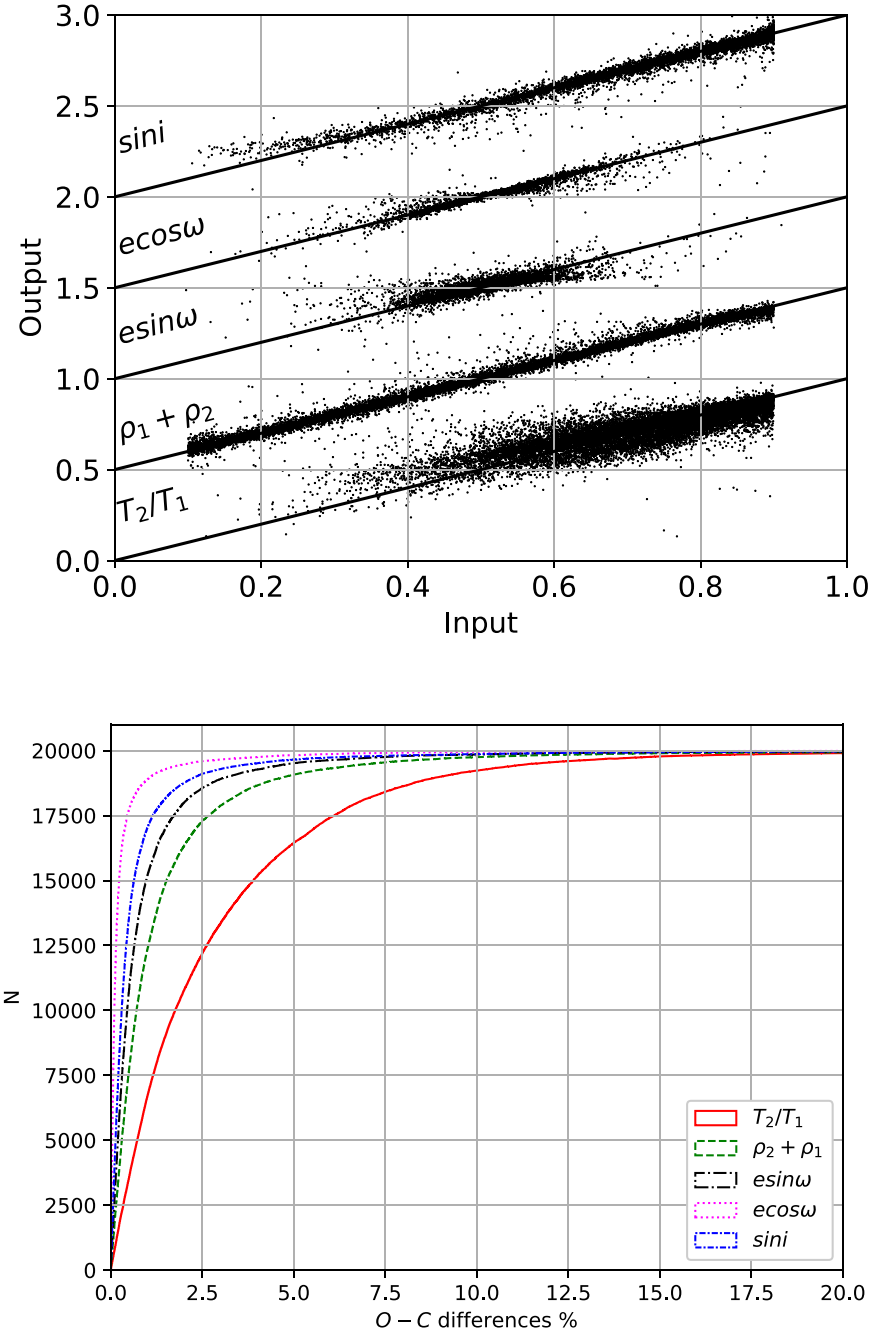

Figure 5. (Top) Actual parameter values of the validation set of 20,000 synthetic LCs vs. the output parameter values calculated from the EBAI code. The values were linearly mapped into the range [0.05–0.9]. The different plotted parameter values were arbitrarily shifted by multiples of 0.5, for clarity. (Bottom) Cumulative distribution of the actual and calculated percentage differences of the parameters $\frac{T_2}{T_1}$, $\rho_2 + \rho_1$, $e \sin\omega$, $e \cos\omega$, and $\sin i$ from the validation set of 20,000 synthetic LCs.

4. Results and Discussion

The sample to be processed using EBAI includes 4683 EBs from CSDR2. The results of the Monte Carlo from the two approaches of Section 2 were combined, and the weighted mean for each parameter was adopted as the final value for each LC. LCs with parameter values out of the parameter range of the training set (specifically, those with $\rho_2 + \rho_1 > 0.5$) were removed from the sample. This resulted in 2281 EBs, out of which 1466 were represented by both TGM and TMPL models; 789 only by TGM models; and 26 only by TMPL models (flag, Table 1). The effect of the previous selection is that the resulting sample is dominated by detached systems. We thus cross-checked our EBs with the findings of Papageorgiou et al. (2018), whereupon 2217 EBs were classified as detached systems.

The derived physical parameters from EBAI are shown in Table 2. The given errors reflect the precision of the corresponding parameter and describe the variation range when EBAI reaches the global solution. The parameter distributions (Figure 6) are in agreement with the results presented by Prša et al. (2008, 2011a) for detached systems. The majority of the systems have the orthogonalized components of eccentricity around 0, corresponding to circular orbits and projected orbits when $\omega = \pm\frac{\pi}{2}$. The inclination and the temperature ratio

Table 2
Physical Parameters of 2281 EBs Derived from EBAI ANN

Name	$\frac{T_2}{T_1}$	$\frac{T_2}{T_1}_{\rm err}$	$\rho_1+\rho_2$	$\rho_1+\rho_{2\rm err}$	$e\sin\omega$	$e\sin\omega_{\rm err}$	$e\cos\omega$	$e\cos\omega_{\rm err}$	$\sin i$	$\sin i_{\rm err}$
CSS_J235856.7+371823	0.8699	0.0466	0.4978	0.0182	0.0388	0.0297	0.0017	0.0117	0.9536	0.0079
CSS_J235715.5+305455	1.0382	0.0524	0.2648	0.0249	0.0020	0.0785	−0.0038	0.0117	0.9883	0.0042
CSS_J235444.8+305751	0.9395	0.0475	0.4750	0.0079	−0.0464	0.0175	0.0104	0.0059	1.0034	0.0013
CSS_J235227.0+395515	1.0128	0.0198	0.4799	0.0129	0.0994	0.0184	−0.0129	0.0049	0.9950	0.0034
CSS_J235151.3+035409	0.6197	0.0690	0.3921	0.0108	0.0486	0.0237	−0.0150	0.0105	0.9993	0.0017
CSS_J235104.0+115651	0.9194	0.0691	0.4504	0.0219	0.0315	0.0249	0.0021	0.0079	0.9790	0.0068
CSS_J234850.3+133300	0.7064	0.1198	0.2656	0.0119	0.0539	0.0609	−0.0154	0.0200	0.9921	0.0013
CSS_J234826.5+271203	0.9434	0.0624	0.3950	0.0186	0.0102	0.0285	0.0004	0.0068	0.9935	0.0036
CSS_J234734.4+203331	0.7487	0.0725	0.3487	0.0115	0.0311	0.0276	0.0033	0.0092	0.9996	0.0012
CSS_J234700.0+180015	0.9843	0.0751	0.2690	0.0247	−0.0829	0.0766	−0.0026	0.0137	0.9887	0.0043
CSS_J234554.3−003131	0.8422	0.0601	0.4496	0.0144	0.0139	0.0220	−0.0032	0.0060	0.9956	0.0032
CSS_J234502.5+415419	1.0216	0.0275	0.4458	0.0169	−0.0277	0.0210	0.0084	0.0093	0.9896	0.0046
CSS_J234348.2+270630	0.9859	0.0555	0.3578	0.0147	0.0223	0.0374	0.0032	0.0062	1.0004	0.0013
CSS_J234331.2−010354	0.9545	0.0781	0.3212	0.0228	−0.0089	0.0685	−0.0020	0.0160	0.9735	0.0045
CSS_J234306.1+060347	0.8122	0.1248	0.1468	0.0127	−0.0183	0.0926	−0.0008	0.0125	0.9997	0.0007
CSS_J233925.0+301419	0.7797	0.0540	0.4295	0.0162	0.0315	0.0321	0.0211	0.0160	0.9784	0.0048
CSS_J233903.3+244754	0.8084	0.0571	0.4860	0.0172	0.0079	0.0213	−0.0004	0.0054	0.9984	0.0033
CSS_J233902.7+364733	0.9697	0.0534	0.4588	0.0218	0.0071	0.0236	−0.0010	0.0075	0.9806	0.0080
CSS_J233834.6+180614	0.7946	0.0797	0.3022	0.0191	−0.0105	0.0553	−0.0016	0.0133	0.9907	0.0035
CSS_J233714.0+324147	0.8830	0.0614	0.4061	0.0203	0.0196	0.0295	0.0011	0.0088	0.9854	0.0049
CSS_J233651.3+353158	0.7951	0.0853	0.3142	0.0123	0.0573	0.0360	−0.0117	0.0087	0.9981	0.0013
CSS_J233608.6+344712	0.9723	0.0514	0.4833	0.0231	0.0056	0.0245	0.0007	0.0078	0.9652	0.0099
CSS_J233511.5+003256	0.7329	0.0506	0.4475	0.0175	0.0220	0.0352	0.0075	0.0258	0.9805	0.0074
CSS_J233440.6+415531	0.9315	0.0759	0.4430	0.0131	0.0423	0.0268	0.0065	0.0063	1.0032	0.0015
CSS_J233313.7+283745	0.9705	0.0544	0.3896	0.0220	0.0047	0.0286	0.0006	0.0079	0.9889	0.0044
CSS_J233159.8+132745	0.9078	0.0680	0.3570	0.0106	0.0166	0.0326	0.0018	0.0079	0.9977	0.0008
CSS_J233133.0+141548	0.9221	0.1008	0.2447	0.0165	0.0741	0.0752	−0.0041	0.0112	0.9976	0.0018
CSS_J233116.3+324003	0.8674	0.0946	0.2676	0.0128	0.0020	0.0543	0.0020	0.0108	0.9993	0.0009

(This table is available in its entirety in machine-readable form.)

distributions are in agreement with the expected distributions for detached systems, with a peak approaching 1.0 and a fast drop-off of the $\sin i$, respectively, in accordance with the geometrical requirements for systems to exhibit eclipses (an edge-on geometrical configuration). In a more detailed look, it is interesting to note that the temperature ratio peaks around ∼0.95, which is in full agreement with the temperature ratio of 257 detached double-lined EBs in the Milky Way collected by Eker et al. (2014). In addition, the error budget of the different parameters shows that the temperature ratio is the more uncertain among the physical quantities obtained in our analysis. Again, this is not an unexpected result, due to the fact that such a ratio is not a clear-cut LC parameter, even though it can be rapidly recovered by an EB model engine such as the one used here. The fractional sum of radii distribution reflects a selection effect, due to the fact that ∼90% of our systems have periods $\lesssim$3 days.

In Table 3, we also present the parameter values from the best-matching template for 1540 out of the 2402 EBs that were found to be outside of the EBAI training limits. For the remaining 862 EBs, either the template fitting was not sufficient enough to provide a reliable solution and was thus removed from the sample during the first visual inspection (179 EBs) or no template was able to match the observed LC.

We remind the reader that some of the parameter values afforded by our analysis could suffer from degeneracies (see Section 3.1), especially for the sample of 1540 EBs with parameters derived solely on the basis of the best-matching template; they should thus be adopted with due caution. However, the values we provide can be used as a starting point in parameter hyperspace for a dedicated model (using, for instance, JKTEBOP[10] or PHOEBE), and/or for statistical purposes. In this sense, Holanda & da Silva (2018) investigated possible discrepancies between the physical parameters derived using EBAI and those obtained using the JKTEBOP code (Southworth et al. 2004a, 2004b). Their analysis was based on 78 EBs randomly sampled from 1400 detached EB systems obtained from the Kepler EB Catalog (Prša et al. 2011a; Slawson et al. 2011; Kirk et al. 2016). Holanda & da Silva showed that, for the 41 EBs with matches in the Kepler EB Catalog, the parameter distributions of $\rho_2+\rho_1$, $e\sin\omega$, and $e\cos\omega$ derived from EBAI and JKTEBOP are statistically consistent with one another. On the other hand, they also found that the EBAI inclination values are systematically underestimated. In particular, they showed that ∼93% of the systems have smaller EBAI-based inclination values, in comparison with those obtained using JKTEBOP, with a median difference of about $-1\overset{\circ}{.}8$.

Last but not least, we performed a systematic search in the literature for dedicated studies on the EBs that are included in our catalog. This resulted in nine EBs (Table 4) for which the derived physical parameters could be directly compared (where available) with our findings. All systems have circular orbits. Unfortunately, the analyses of most of these systems in the literature are based solely on photometric data. Table 4 shows a comparison of the parameter values from the literature versus the EBAI results. The case of the EB system CSS_J152154.8

[10] JKTEBOP code is available at http://www.astro.keele.ac.uk/jkt/codes/jktebop.html.

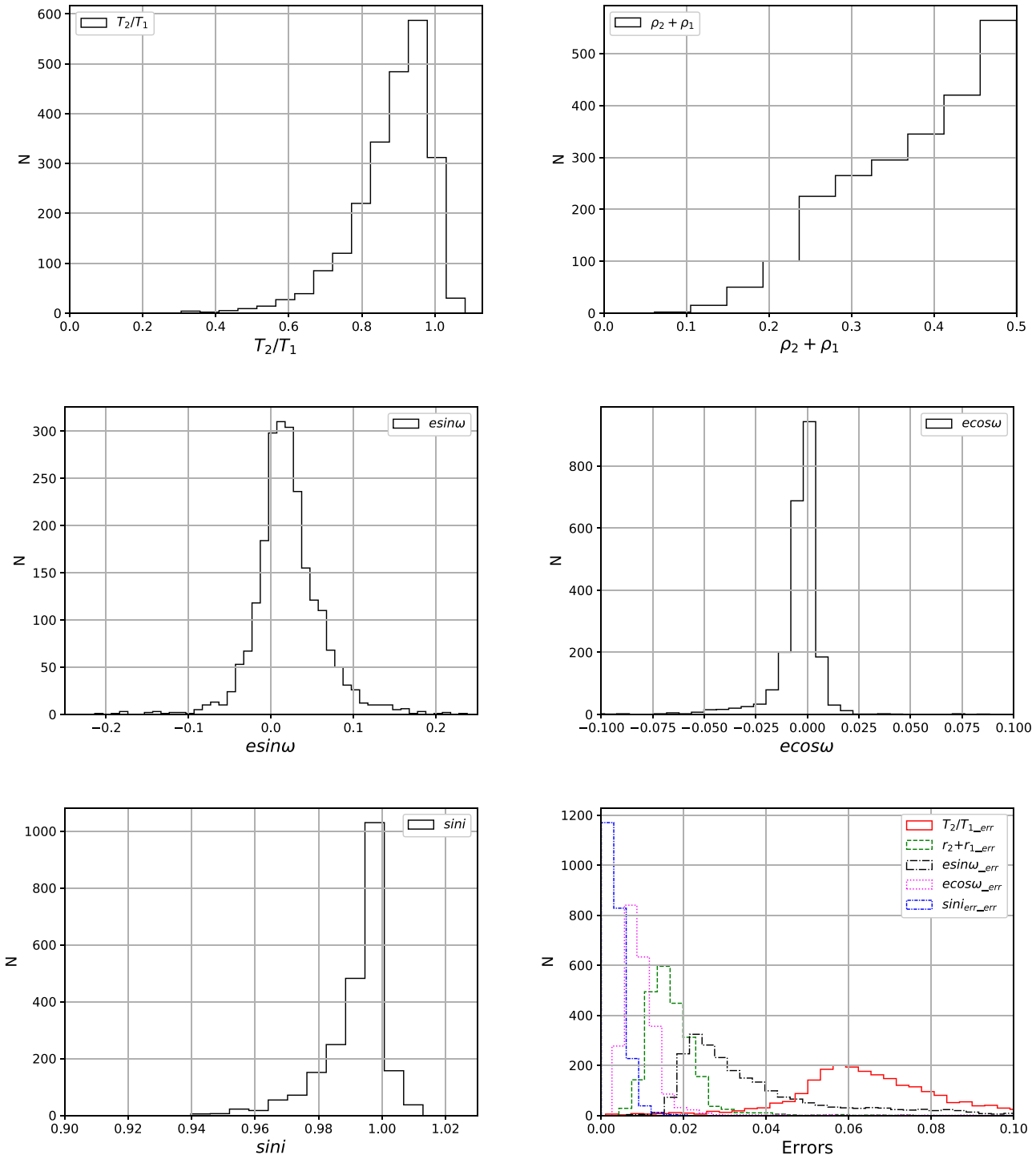

Figure 6. Distribution of the derived parameters $\frac{T_2}{T_1}$ (top left), $\rho_2 + \rho_1$ (top right), $e \sin\omega$ (middle left), $e \cos\omega$ (middle right), and $\sin i$ (bottom left) for 2281 CSS EBs from EBAI. The relative error budget corresponding to each of these parameters, as listed in Table 2, is shown in the bottom right panel.

+335609 (GU Boo; Windmiller et al. 2010) became a benchmark for our comparisons. Windmiller et al. (2010), after an extensive analysis (global solution, error analysis) based on follow-up photometric data, historical photometric LCs, and spectroscopic data, derived the absolute parameters of the system. The comparison of our solution with their results shows excellent agreement (less than ∼5% percentage difference in the derived parameters). The majority of the systems are in very good agreement with our results (less than ∼10% percentage difference). Again, larger deviations were found in the temperature ratios, especially in systems with shallow eclipses such as CSS_J142920.9+320804 (SU Boo; Zasche et al. 2014) and CSS_J094749.7+125902 (UU Leo; Yang 2013).

Our analysis revealed interesting subsamples of EBs. About 27% of the total sample analyzed with the EBAI ANN are well-detached EBs with deep eclipses (more than 35% decrease in brightness during the eclipses). These systems could be excellent candidates for follow-up observations in order to derive accurate absolute physical parameters (stellar masses,

Table 3
Physical Parameters of 1540 EBs Derived from the Matching Templates

Name	ID	R.A. (h:m:s)	Decl. (°: ′: ″)	$\frac{r_2}{r_1}$	$\rho_1 + \rho_2$	$e \sin \omega$	$e \cos \omega$	$\sin i$	Flag
CSS_J235816.7+293325	1129113035231	23:58:16.72	+29:33:25.3	0.7103	0.6778	0.0005	−0.0001	0.9960	Template
CSS_J234819.9+344833	1135106027985	23:48:19.93	+34:48:33.9	0.4972	0.5038	0.0000	0.0002	0.9924	Template
CSS_J234439.7+055255	1107126005261	23:44:39.77	+05:52:55.8	0.8819	0.7793	−0.0001	0.0001	0.9280	Template
CSS_J234116.3+392234	1138102085374	23:41:16.38	+39:22:34.6	0.5424	0.5953	0.0042	−0.0167	0.9703	Template
CSS_J234042.4+045812	1104127044669	23:40:42.43	+04:58:12.1	0.5910	0.6348	0.0003	0.0002	0.9269	Template
CSS_J233905.2+385936	1138102071715	23:39:05.24	+38:59:36.4	0.7025	0.5373	0.0173	0.0071	0.9909	Template
CSS_J233637.3+383526	1138102058861	23:36:37.31	+38:35:26.6	0.6882	0.5942	0.0003	0.0069	0.9821	Template
CSS_J233500.6−151319	1015122034530	23:35:00.61	−15:13:19.8	0.4606	0.5320	−0.0006	−0.0011	0.9786	Template
CSS_J233441.0+112836	1112124004170	23:34:41.02	+11:28:36.7	0.6654	0.6605	−0.0014	0.0035	0.9799	Template
CSS_J233420.4+401639	1140098026839	23:34:20.44	+40:16:39.6	0.5560	0.5273	0.0036	−0.0150	0.9756	Template
CSS_J233123.7+410814	1140098056995	23:31:23.78	+41:08:14.2	0.5287	0.5822	−0.0024	0.0041	0.9643	Template
CSS_J233115.5−105959	1009125005527	23:31:15.58	−10:59:59.2	0.7874	0.6640	−0.0032	0.0087	0.9646	Template
CSS_J233036.2+253604	1126114005561	23:30:36.25	+25:36:04.9	0.7094	0.6238	0.0023	0.0096	0.9779	Template
CSS_J232940.8+164908	1115122060487	23:29:40.80	+16:49:08.7	0.7060	0.5688	0.0056	0.0094	0.9272	Template
CSS_J232707.5+335936	1135104004273	23:27:07.51	+33:59:36.7	0.7176	0.5365	0.0003	−0.0006	0.9825	Template
CSS_J232515.1+361202	1135104074803	23:25:15.10	+36:12:02.5	0.7687	0.6131	0.0097	0.0108	0.9460	Template
CSS_J232500.9+310349	1132108001462	23:25:00.91	+31:03:49.1	0.9133	0.5778	0.0049	−0.0012	0.9761	Template
CSS_J232328.8+292554	1129111033401	23:23:28.80	+29:25:54.3	0.6967	0.7467	0.0000	0.0002	0.9351	Template
CSS_J232320.6+371417	1138101018164	23:23:20.60	+37:14:17.6	0.6667	0.5364	−0.0016	−0.0067	0.9865	Template
CSS_J232034.2−031415	1004125046646	23:20:34.23	−03:14:15.9	0.6317	0.7687	0.0027	0.0024	0.9050	Template
CSS_J231954.6+260657	1126113019830	23:19:54.67	+26:06:57.0	0.7568	0.5974	−0.0087	−0.0005	0.9808	Template
CSS_J231817.2+402345	1140097031668	23:18:17.28	+40:23:45.9	0.7665	0.4211	0.0136	−0.0097	0.9993	Template
CSS_J231741.6+041426	1104125028483	23:17:41.67	+04:14:26.1	0.6552	0.5944	−0.0000	−0.0002	0.9758	Template
CSS_J231552.6+275047	1126113067214	23:15:52.69	+27:50:47.5	0.6564	0.5720	−0.0001	−0.0001	0.9991	Template
CSS_J231538.7+225837	1123115010343	23:15:38.71	+22:58:37.8	0.8076	0.5199	−0.0066	−0.0173	1.0000	Template
CSS_J231511.0+275607	1126113069728	23:15:11.07	+27:56:07.4	0.7249	0.5700	−0.0015	0.0031	0.9978	Template
CSS_J231207.2+304611	1129110073683	23:12:07.24	+30:46:11.8	0.6472	0.5160	−0.0091	0.0069	0.9919	Template
CSS_J231115.6+340643	1135103008319	23:11:15.61	+34:06:43.9	0.5846	0.7326	−0.0000	0.0028	0.9719	Template
CSS_J231109.2+102705	1109123044436	23:11:09.21	+10:27:05.7	0.6844	0.6256	0.0003	−0.0008	0.9988	Template
CSS_J230924.0+263058	1126112031484	23:09:24.03	+26:30:58.6	0.5326	0.5147	0.0068	0.0004	0.9610	Template

(This table is available in its entirety in machine-readable form.)

Table 4
Comparison of EBAI Results with Dedicated Studies on Nine EBs Found in the Literature

Name	$\frac{r_2}{r_1}$ [a]	$\frac{r_2}{r_1}$ [b]	$\rho_1 + \rho_2$ [a]	$\rho_1 + \rho_2$ [b]	i (°) [a]	i (°) [b]	$(\frac{r_2}{r_1})$(%)	$(\rho_1 + \rho_2)$(%)	i (°)(%)	References
CSS_J152154.8+335609	0.960	0.970	0.427	0.447	90.00	88.24	1.02	4.42	2.00	Windmiller et al. (2010)
CSS_J160727.8+121359	0.991	0.973	0.432	0.429	88.92	85.46	1.90	0.84	4.05	Zhang et al. (2015)
CSS_J165241.7+124905	0.782	0.900	0.418	0.435	84.01	87.46	13.10	3.90	3.94	Zhang (2012)
CSS_J090859.3+093541	0.643	0.615	0.417	0.499	90.00	87.96	4.52	16.34	2.32	Lacy (2004)
CSS_J142920.9+320804	0.814	0.602	0.394	0.423	86.72	83.14	35.21	6.75	4.31	Zasche et al. (2014)
CSS_J094749.7+125902	0.786	0.600	0.473	0.465	82.12	87.96	31.01	1.84	6.63	Yang (2013)
CSS_J092128.3+332558	0.976	N/A	0.425	0.530	78.05	73.46	N/A	19.80	6.25	Lee & Lin (2017)
CSS_J074118.8+311434	0.988	N/A	0.212	0.240	83.56	83.46	N/A	11.60	0.13	Lee & Lin (2017)
CSS_J072108.8+344808	1.000	N/A	0.336	0.310	85.15	89.85	N/A	8.42	5.24	Lee & Lin (2017)

Notes.
[a] EBAI.
[b] Literature.

radii, etc.). By crossmatching our catalog with the catalog published in Papageorgiou et al. (2018), we found, in particular, that ∼22% of the systems are good low-mass EB system candidates. Furthermore, ∼3% of the systems show eccentricities greater than 0.05 and deep eclipses. These EBs could be good candidates for eccentric EB studies and for a further analysis of their orbits (apsidal motion studies).

5. Conclusions

This paper presents an estimate of the main physical parameters of 2281 CSS EBs, based on the EBAI ANN. For our training set, we generated theoretical LCs via a Monte Carlo–based script utilizing the PHOEBE-scripter, which samples EB parameter values according to prior distribution functions. The use of TMPL fitting and TGM modeling in the preprocessing of the observed data is novel to our analysis. The general statistical characteristics of the derived parameters are

similar to those characterizing the EB systems in the first release of the Kepler catalog of detached EBs (Prša et al. 2011a) obtained by the method of neural networks and also with the catalog of parameter values for 257 detached double-lined EBs (Eker et al. 2014) obtained by the traditional method. In addition, the TMPL class labels are in agreement, in 84% of the cases, with the classification given by Papageorgiou et al. (2018). Due to the selection biases inherent to our EB sample, our database can serve to investigate individual systems at the edge of the general parameter distributions that characterize binary star systems.

A.P. and M.C. gratefully acknowledge the support provided by Fondecyt through grants Nos. 3160782 and 1171273. Additional support for this project is provided by the Ministry for the Economy, Development, and Tourism's Millennium Science Initiative through grant IC 120009, awarded to the Millennium Institute of Astrophysics (MAS); by Proyecto Basal AFB-170002; and by CONICYT's PCI program through grant DPI20140066. We are grateful to Dr. Andrej Prša for his helpful comments and suggestions. The Monte Carlo script in the PHOEBE-scripter is based on the script that was kindly provided by Dr. Andrej Prša.

This work made use of data products from the CSS survey. The CSS survey is funded by the National Aeronautics and Space Administration under grant No. NNG05GF22G issued through the Science Mission Directorate Near-Earth Objects Observations Program. The CRTS survey is supported by the US National Science Foundation under grants AST-0909182, AST-1313422, AST-1413600, and AST-1518308.

The data processing have been supported by the Geryon 2 supercomputer hosted at the Institute of Astrophysics and Astro-Engineering Center, Pontificia Universidad Católica de Chile.

Software: EBAI (Prša et al. 2008), PHOEBE-scripter (Prša & Zwitter 2005).

ORCID iDs

Athanasios Papageorgiou https://orcid.org/0000-0002-3039-9257
Márcio Catelan https://orcid.org/0000-0001-6003-8877
S. G. Djorgovski https://orcid.org/0000-0002-0603-3087

References

Bertin, E., & Arnouts, S. 1996, A&AS, 117, 393
Chen, X., Wang, S., Deng, L., de Grijs, R., & Yang, M. 2018, ApJS, 237, 28
Drake, A. J., Catelan, M., Djorgovski, S. G., et al. 2013, ApJ, 763, 32
Drake, A. J., Djorgovski, S. G., Mahabal, A., et al. 2009, ApJ, 696, 870
Drake, A. J., Graham, M. J., Djorgovski, S. G., et al. 2014, ApJS, 213, 9
Eker, Z., Bilir, S., Soydugan, F., et al. 2014, PASA, 31, e024
Graczyk, D., Pietrzyński, G., Thompson, I. B., et al. 2014, ApJ, 780, 59
Graham, M. J., Djorgovski, S. G., Drake, A. J., et al. 2017, MNRAS, 470, 4112
Guinan, E. F., Prša, A., Devinney, E. J., & Engle, S. G. 2009, in ASP Conf. Ser. 404, The Eighth Pacific Rim Conf. Stellar Astrophysics: A Tribute to Kam-Ching Leung, ed. B. Soonthornthum (San Francisco, CA: ASP), 361
Hełminiak, K. G., Devor, J., Minniti, D., & Sybilski, P. 2013, MNRAS, 432, 2895
Holanda, N., & da Silva, J. R. P. 2018, MNRAS, 478, 1272
Kirk, B., Conroy, K., Prša, A., et al. 2016, AJ, 151, 68
Lacy, C. H. S. 2004, IBVS, 5499, 1
Larson, S., Beshore, E., Hill, R., et al. 2003, BAAS, 35, 36.04
Layden, A. C. 1998, AJ, 115, 193
Lee, C.-H., & Lin, C.-C. 2017, RAA, 17, 15
Mikulášek, Z. 2015, A&A, 584, A8
Mowlavi, N., Lecoeur-Taïbi, I., Holl, B., et al. 2017, A&A, 606, A92
Papageorgiou, A., Catelan, M., Christopoulou, P.-E., Drake, A. J., & Djorgovski, S. G. 2018, ApJS, 238, 4
Pietrzyński, G., Graczyk, D., Gieren, W., et al. 2013, Natur, 495, 76
Prša, A., Batalha, N., Slawson, R. W., et al. 2011a, AJ, 141, 83
Prša, A., Guinan, E. F., Devinney, E. J., et al. 2008, ApJ, 687, 542
Prša, A., Pepper, J., & Stassun, K. G. 2011b, AJ, 142, 52
Prša, A., & Zwitter, T. 2005, ApJ, 628, 426
Slawson, R. W., Prša, A., Welsh, W. F., et al. 2011, AJ, 142, 160
Southworth, J., Maxted, P. F. L., & Smalley, B. 2004a, MNRAS, 351, 1277
Southworth, J., Zucker, S., Maxted, P. F. L., & Smalley, B. 2004b, MNRAS, 355, 986
Udalski, A., Szymanski, M., Kaluzny, J., Kubiak, M., & Mateo, M. 1992, AcA, 42, 253
van Hamme, W. 1993, AJ, 106, 2096
Windmiller, G., Orosz, J. A., & Etzel, P. B. 2010, ApJ, 712, 1003
Wyrzykowski, L., Udalski, A., Kubiak, M., et al. 2003, AcA, 53, 1
Yang, M., Zhang, H., Wang, S., et al. 2015, ApJS, 217, 28
Yang, Y.-G. 2013, RAA, 13, 1471
Zasche, P., Wolf, M., Uhlař, R., & Kučáková, H. 2014, AJ, 147, 130
Zhang, B., Qian, S.-B., Liao, W.-P., et al. 2015, NewA, 41, 37
Zhang, L.-Y. 2012, RAA, 12, 433